Bulletin of Volcanology, 80:13, doi:10.1007/s00445-017-1188-7.

Formation of a spatter-rich pyroclastic density current deposit in a Neogene sequence of trachytic—mafic igneous rocks at Mason Spur, Erebus volcanic province, Antarctica

Martin, A. P.[1], Smellie, J. L.[2], Cooper, A. F.[3], Townsend, D. B.[4]

[1] GNS Science, Private Bag 1930, Dunedin, New Zealand. a.martin@gns.cri.nz
[2] University of Leicester, Department of Geology, University Road, Leicester LE1 7RH, UK
[3] Department of Geology, University of Otago, P.O. Box 56, Dunedin, New Zealand
[4] GNS Science, PO Box 30-368, Lower Hutt, New Zealand

Abstract

Erosion has revealed a remarkable section through the heart of a volcanic island, Mason Spur, in the southwestern Ross Sea, Antarctica, including an unusually well exposed section of caldera fill. The near-continuous exposure, 10 km laterally and >1 km vertically, cuts through Cenozoic alkalic volcanic rocks of the Erebus volcanic province (McMurdo Volcanic Group) and permits the study of an ancient volcanic succession that is rarely available due to subsequent burial or erosion. The caldera filling sequence includes an unusual trachytic spatter-rich lapilli tuff (ignimbrite) facies that is particularly striking because of the presence of abundant black fluidal, dense juvenile spatter clasts of trachytic obsidian up to 2m long supported in a pale cream-coloured pumiceous lapilli tuff matrix. Field mapping indicates that the deposit is an ignimbrite and, together with petrological considerations, it is suggested that mixing of dense spatter and pumiceous lapilli tuff in the investigated deposit occurred during emplacement, not necessarily in the same vent, with the mixed fragmental material emplaced as a pyroclastic density current. Liquid water was not initially present but a steam phase was probably generated during transport and may represent water ingested during passage of the current as it passed over either wet ground (possibly puddled), a stream, shallow lake or possibly snow. Well exposed caldera interiors are uncommon and that at Mason Spur is helping understand eruption dynamics associated with a complex large island volcano. The results of our study should help to elucidate interpretations of other, less well exposed pyroclastic density current deposits elsewhere in Antarctica and globally.

Keywords *Explosive volcanism; ignimbrite; Lapilli tuff; McMurdo Volcanic Group Pyroclastic Density Current; Trachytic spatter*

Introduction

At a number of localities worldwide, pyroclastic deposits have been found that contain both dense fluidal spatter and a pumiceous matrix. Examples include Antarctica (Elliot and Hanson 2001 (basalt)), Italy (Trigila and Walker 1986 (trachyte); Scarpati et al. 1993 (trachyte); Giannetti and Luongo 1994 (trachyandesite and trachyte); Perrotta and Scarpati 1994 (trachyte)), Greece (Mellors and Sparks 1991 (andesitic)), St. Kitts (Roobol et al. 1987 (basaltic andesite)), USA (Valentine et al. 2000 (mafic andesite)), Vanuatu ((Allen 2005 (andesite)) and the United Kingdom (Kokelaar et al. 2007 (andesitic)). Previously described deposits mostly describe lava spatter and are generally glass-free (c.f. Rosi et al. 1996). Understanding the eruptive conditions responsible for mixing together these two very different clast types has implications for volcanic hazard assessment and for interpreting the dynamics and depositional processes of explosive eruptions. We use exceptional outcrops at Mason Spur, Antarctica, to shed light on this issue. At Mason Spur, a trachytic unit contains prominent black obsidian ribbon-like clasts (dense fluidal spatter) dispersed in cream-coloured pumice lapilli and ash. The obsidian spatter is especially unusual, as it shows textural evidence for ductile deformation, pervasive brittle fracturing and complete disintegration to obsidian lapilli not described elsewhere. The studied deposits are part of an intra-caldera sequence exposed in 1000 m-high crags at Mason Spur, which is a dissected volcanic island within the alkalic, Cenozoic McMurdo Volcanic Group (Figs. 1 and 2). This work builds on preliminary descriptions of the physical volcanology of Mason Spur (e.g. Wright-Grassham 1987; Martin et al. 2013). In this paper, the deposit characteristics at Mason Spur are presented and the mechanisms for mixing these two very different clast types together are discussed, with a preferred model presented.

Geological Setting

This paper describes a highly distinctive trachytic deposit containing conspicuous large ribbon-like clasts of obsidian that crops out at Windscoop Bluff, at the eastern end of Mason Spur. Mason Spur forms part of the Mt Morning volcanic field, which is within the McMurdo Volcanic Group, a geographically widespread group of sodic alkaline volcanoes that crop out extensively along the western margin of the West Antarctic rift system where it abuts the Transantarctic Mountains (Kyle 1990). The volcanism extends over a north—south distance of c. 1800 km between Mt Early and Cape Adare (Fig. 1a). It is genetically related to extension in the West Antarctic rift system, a major pan-Antarctic extensional feature caused primarily by Cenozoic rifting and whose dimensions are comparable with the East African Rift and the Basin and Range Province of USA (LeMasurier 1990).

The obsidian-bearing deposit that is the focus of this paper occurs within a prominent stratigraphic unit that forms the exposed base of Mason Spur. This basal unit is composed of massive ash-poor lithic breccias and lapilli tuff (ignimbrite) with trachytic compositions (Fig. 2). Mason Spur is a north-east trending linear bluff reaching a height of > 1300 m above sea level, with exposure in mainly southeast- to southwest-facing crags and along cliff tops (Fig. 2). The locality is remarkable for the extensive exposure of Cenozoic igneous rocks in sections individually a few hundred metres high, with a cumulative exposure of around 1000 m in stratigraphic thickness. Multiple generations of hypabyssal and volcanic rock units are traceable for a distance of c. 10 km (Fig. 2). The cliffs are crosscut by numerous normal faults and dykes and draped by extensive colluvium. At the nearby larger and higher Mt Morning eruptive centre (Fig. 1b), petrological studies have identified an early, strongly alkalic Mason Spur Lineage and a late, mildly alkalic Riviera Ridge Lineage (Martin et al. 2013). Volcanic outcrops at Mason Spur are dominated by rocks from the early Mason Spur Lineage, which have been dated at between 12.9 ± 0.1 and 11.4 ± 0.2 Ma, although Mason Spur Lineage exposed to the north of Mason Spur (not necessarily physically connected to the Mason Spur volcano) extends back to 18.7 ± 0.3 Ma and 24.1 Ma (Martin and Cooper, 2010; Martin et al. 2010). Mason Spur Lineage rocks are unconformably overlain by the younger Riviera Ridge Lineage (≤ 6.13 ± 0.20 Ma), exposures of which are restricted mainly to cliff tops and rare cross-cutting dykes. The exposed, intra-caldera Mason Spur Lineage rocks are predominantly trachytic and were emplaced by explosive mechanisms, as intrusions and as minor lava flows; unconformably overlying basanitic rocks are mainly lavas and associated minor scoria cones. The Riviera Ridge Lineage rocks occur as scoria and spatter cones, lavas and minor tuff cones. Caldera-filling deposits and ignimbrites are very rare in Antarctic volcanoes, with only two other locations known (e.g. Panter et al. 1994; Smellie and López-Martínez 2002; Martí et al. 2013).

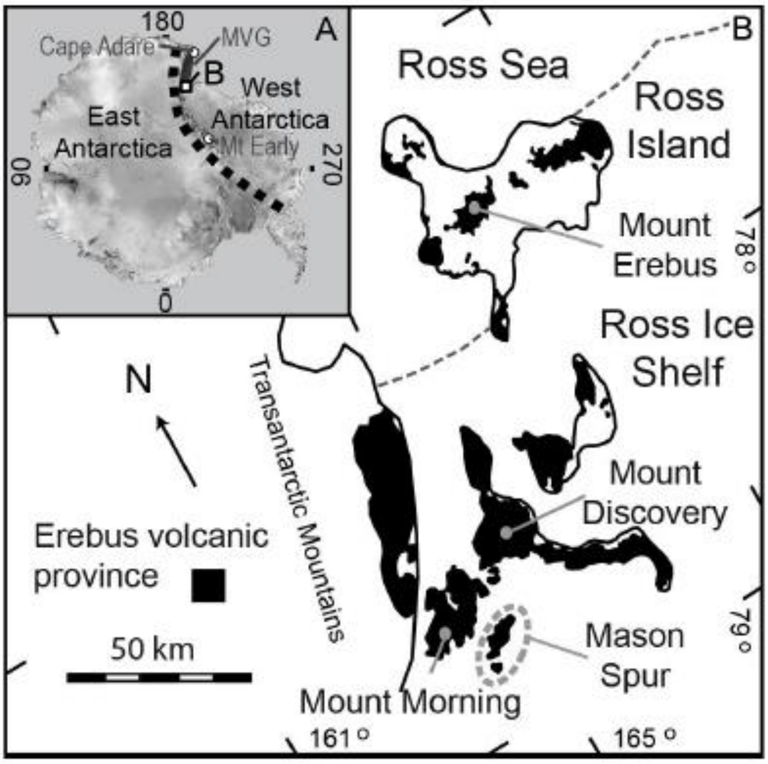

Fig. 1 Locality diagram of Mason Spur, Antarctica. **a** the Antarctic continent showing the approximate position of the Transantarctic Mountains (dashed lines), the McMurdo Volcanic Group (MVG) and the position of b. **b** Erebus volcanic province showing rock outcrop distribution and the locality of Mason Spur relative to other places mentioned in the text.

Methodology and terminology

The volcaniclastic rock classification used here follows the recommendations of Branney and Kokelaar (2002) and White and Houghton (2006). All rock descriptions are based upon field observations and petrography. All rock descriptions are based upon field observations and petrography. Further rock descriptions of the Mason Spur volcanic complex are available in Martin (2009) and Martin et al. (2013). Specimens are housed in the University of Otago collection, New Zealand. X-ray fluorescence (XRF) whole rock analyses were performed at the University of Otago following procedures outlined in Martin et al. (2015). Obsidian compositions were determined by analysing hand-picked obsidian fragments mounted in epoxy resin briquettes using a JEOL JXA-8600 electron microprobe (EMP) at Otago University, operated with accelerating voltage 15kV, current 1μA and beam diameter 20 μm. The analyses were performed in energy dispersive mode and a standard ZAF correction was applied to all data. Image analysis software (ImageJ) was used to measure clast characteristics at the outcrop scale by digitising field photographs of three key sections then using these data to determine average clast length, width, orientation and percentage of total outcrop. Image analysis followed procedures available online at http://rsbweb.nih.gov.

In hand specimen and thin section, vesicle density and shape were visually estimated using the general categories of Houghton and Wilson (1989).

Results

The deposit is described from a vertical section through Windscoop Bluff, which is a southwest-facing series of cliffs, 1 km in length, offering near-continuous exposure from 230 m to > 1000 m above sea level. A simplified composite section through Windscoop Bluff is shown in Fig. 3 (location shown in Fig. 2). The depicted succession comprises Mason Spur Lineage rocks, which at Windscoop Bluff may be subdivided into two members: an earlier trachytic *pyroclastic member* that is extensively intruded (*intrusive member*) and overlain by a younger trachyte lava flow (not discussed here). The section is succeeded unconformably by basanite lava flows and scoria cone deposits (also Mason Spur Lineage) then by better-formed basanite scoria cones and a phonolite dome (Riviera Ridge Lineage; not shown in the sketched section). The trachytic pyroclastic member consists of at least two pyroclastic lithofacies (A, B), which are described below.

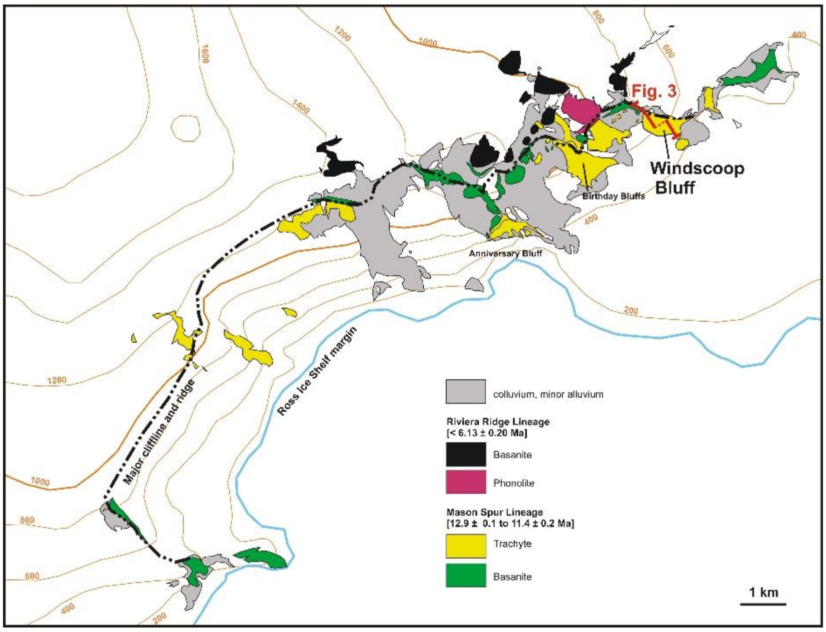

Fig. 2 Simplified geological map of Mason Spur. The approximate position of the idealised section of Fig. 3 is shown in red. Contours are in metres

Trachytic pyroclastic member

Lithofacies A [trachytic lapilli tuff]

Deposits of lithofacies A dominate the outcrop at Windscoop Bluff. It is composed of mainly massive, to rarely diffusely stratified, pumiceous lapilli tuff many tens of metres thick that extends laterally for hundreds of metres (Fig. 4a). In hand specimen, medium lapilli (≤ 1 cm) of pumice (≥ 60%), minor black obsidian (< 10%) and lithic clasts (usually <1% but may form concentrated lenses and beds (Fig. 4a); ≤ 1 mm; aphanitic trachytic lava with abundant pilotaxitic microlites) are supported in a tuff matrix. (c. 25%; Fig. 4b). Decimetre-size flattened to oblate, pale grey, vesicular fiammé-like bombs (usually < 1%) are present in a few places and may form clusters a few metres thick and ash-coated lapilli are sometimes abundant but occurrences are rare (Fig. 4b, c). The matrix and pumice lapilli are cream coloured when fresh, with the black obsidian fragments locally giving the rock a flecked appearance. Tube pumice dominates the juvenile lapilli. The obsidian in thin section is colourless to pale yellow under plane polarised light. Rare anhedral (broken) alkaline feldspar and aegerine-augite (≤ 1 mm) phenocrysts are also present. The matrix is formed of fine and coarse ash-size angular fragments of broken pumice (mainly tube pumice) and shards, and although pervasive, a very finely crystalline clay alteration of the original glass masks the clast shapes in places (Fig. 4d).

Lithofacies B [trachytic spatter-rich lapilli tuff]

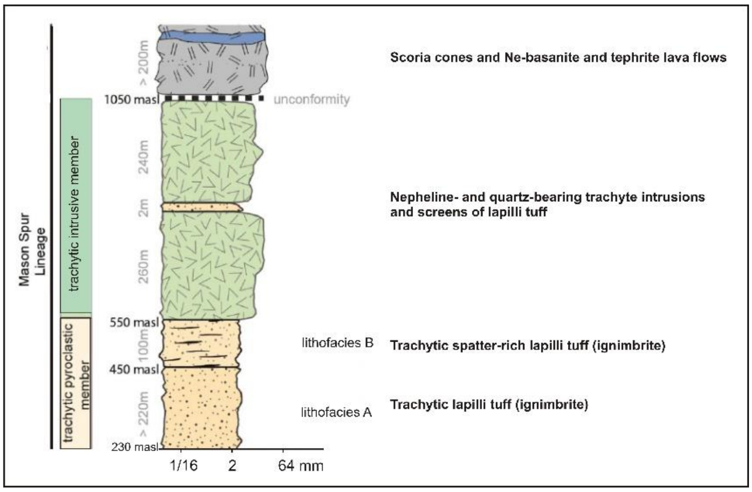

Fig. 3 An idealised stratigraphic section through Mason Spur at Windscoop Bluff with brief descriptions given. The location of the section is shown in Fig. 2. *masl*, metres above sea level

This lithofacies (Fig. 3) is a volumetrically minor part of the succession at Windscoop Bluff, occurring at a single known locality. It is probably the deposit described by Wright-Grassham (1987, p. 42) as '*massive, matrix-rich, obsidian-bearing lapilli tuff containing lobes of trachytic lava, with spalling obsidian rinds*' within her local stratigraphical unit MS5. The lithofacies is massive, cream coloured and poorly sorted, dominated by pumiceous lapilli similar to lithofacies A. It is distinguished by visually striking, highly elongate black obsidian clasts up to 2 m in length with a vitreous lustre and conchoidal fracture, supported in a pale cream-coloured matrix of pumice lapilli and minor ash (Fig. 5a). Lithofacies B is exposed for c. 150 m laterally and is at least 80 m thick. It rests on lapilli tuffs of lithofacies A with a sharp gently undulating contact that becomes indistinct up-dip to the northwest. The upper contact of lithofacies B is intrusive, composed of brownish-grey irregularly shaped intrusions

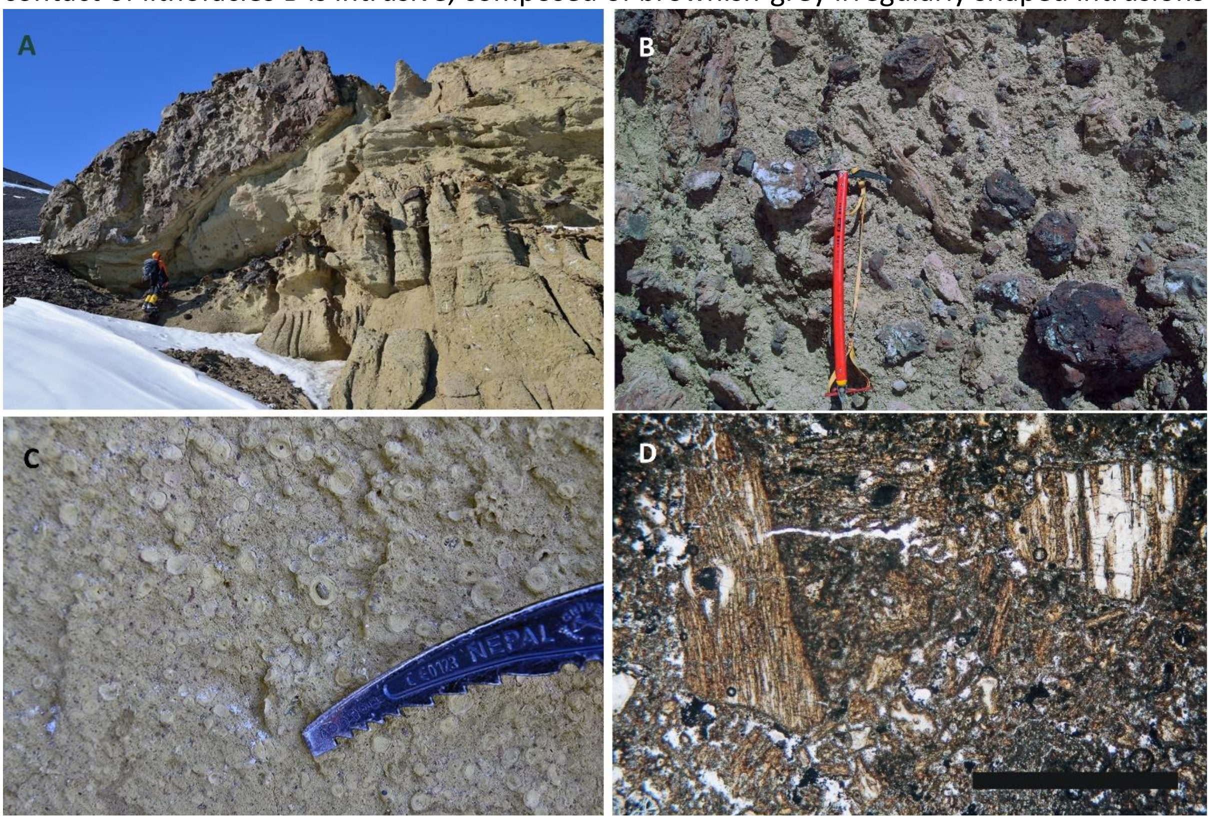

Fig. 4 Views of lithofacies A. **a** General view of lithofacies A outcrop. Although the lithofacies is mainly composed of massive pumice lapilli tuff many tens of metres thick and extending laterally for hundreds of metres, it is partly diffusely stratified at this locality. Numerous blocks of trachytic lava and fewer vesicular bombs form the diffuse dark layer to the right of the person and also the prominent thick bed at upper left. **b** Close view showing flattened bombs and lithic clasts (brown trachytic lava; C) in pale-coloured pumiceous lapilli and ash matrix. The photograph was taken top right of the figure shown in A and is unusually rich in accessory lava blocks.Ice axe is 70 cm long. **c** Abundant ash-coated lapilli. Ice axe head is c. 12 cm long. **d** Photomicrograph (plane polarised light) showing angular tube pumice and abundant fine ash formed of the same.

of the trachytic intrusive member (Figs 3 and 5a); similar intrusions are also present within lithofacies A. The basal 1-2 m of lithofacies B is marked by an absence of obsidian clasts larger than 1 cm, but otherwise there is no vertical variation in the abundance and size of the large obsidian clasts up through the deposit. The lithofacies is mainly composed of finely vesicular juvenile medium lapilli (2 mm to 1 cm in diameter) together with a small proportion (typically c. 1 %) of slightly flattened pumiceous rags up to 5 cm across variably clast- to matrix-supported in c. 10-20 % ash matrix (Fig. 5b). Diffuse-margined ‘domains’ with c. 10-20 % angular fresh obsidian fragments are also common (Fig. 5c). Pumice clast vesicularity is high to very high (≥ 70 %) and many are extensively strained tube pumice; the pumices and obsidians are crystal free and even lack crystallites (Fig. 5d).

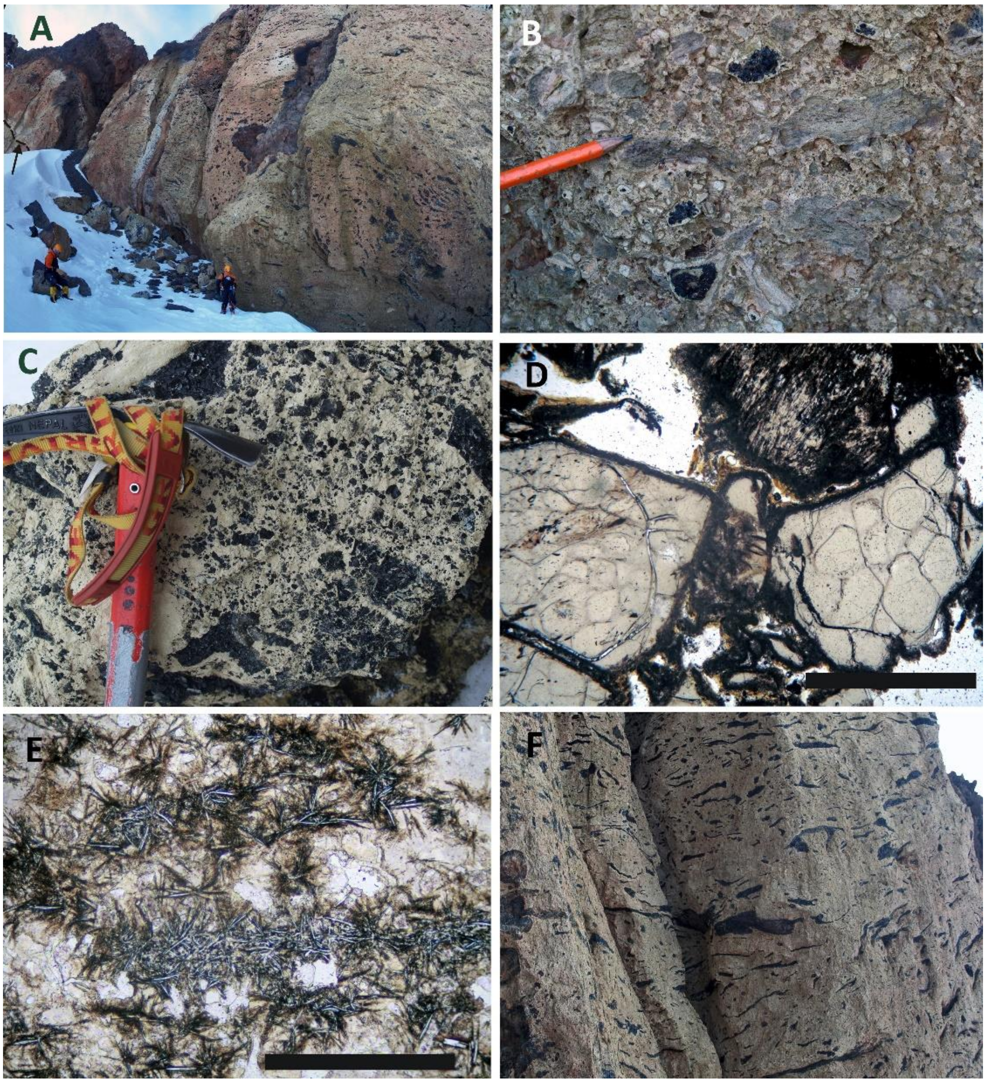

Fig. 5 Views of lithofacies B. **a** Typical view of spatter-rich lapilli tuff; the upper contact is intrusive and an amoeboid intrusion is shown near the centre of the outcrop (dark grey and brown rocks); the sharp uneven erosive basal surface is visible at upper left (arrowed), dipping c. 12° east. **b** Close view showing flattened ragged bombs, abundant pumice and scarcer black obsidian lapilli. The pencil is 5 cm long. **c** Diffuse domain rich in angular obsidian fragments; compare the abundance of obsidian lapilli present with their paucity in Fig. 5B. **d** Photomicrograph (plane polarised light) of obsidian-rich domain showing colourless angular nonvesicular obsidian clasts with perlitic fractures and tube pumice; the obsidians and pumices are crystal free. The scale bar is 1 mm long. **e** Photomicrograph (plane polarised light) showing trails of decussate crystallites in obsidian

spatter caused by devitrification. The scale bar is 0.5 mm long. **f** Close view of the spatter-rich lapilli tuff showing prominent parallel spatter orientation; note how most of the obsidians are extremely thin and also their disk-like shapes revealed by the uneven outcrop surface (ribbon-like in cross section); the obsidians also have relatively smooth featureless surfaces. The view shown is c. 2 m high. **g** View of an amoeboid coeval intrusion with overlying spatter deflected upward, suggesting localised gas fluidisation from within the ignimbrite or fluidization of an unconsolidated wet or moist host deposit. The view shown is c. 7 m high. **h** A fluidal obsidian spatter clast folded in two; there are no fractures at the hinge. The penknife is 4 cm long. **i.** Recurved plastically deformed obsidian ribbon also showing brittle fracturing and local brecciation; note abundant black blocky obsidian lapilli mixed with pale pumiceous lapilli tuff (contrast with Fig. 5h); the obsidian lapilli probably formed by disintegration of obsidian spatter. The ice axe is c. 35 cm long. **j** Obsidian ribbon broken and extended into a trail of angular fragments. The ice axe (inset) is c. 35 cm long. **k** Close view of obsidian ribbon showing pervasive small-scale jigsaw-fit fracturing. The pencil is 4 cm long. **l** Obsidian spatter clast with delicate, finger-like and wispy terminations; note also the scattered blocky obsidian lapilli, derived by disintegration of other obsidian spatter. The ice axe is c. 25 cm long.

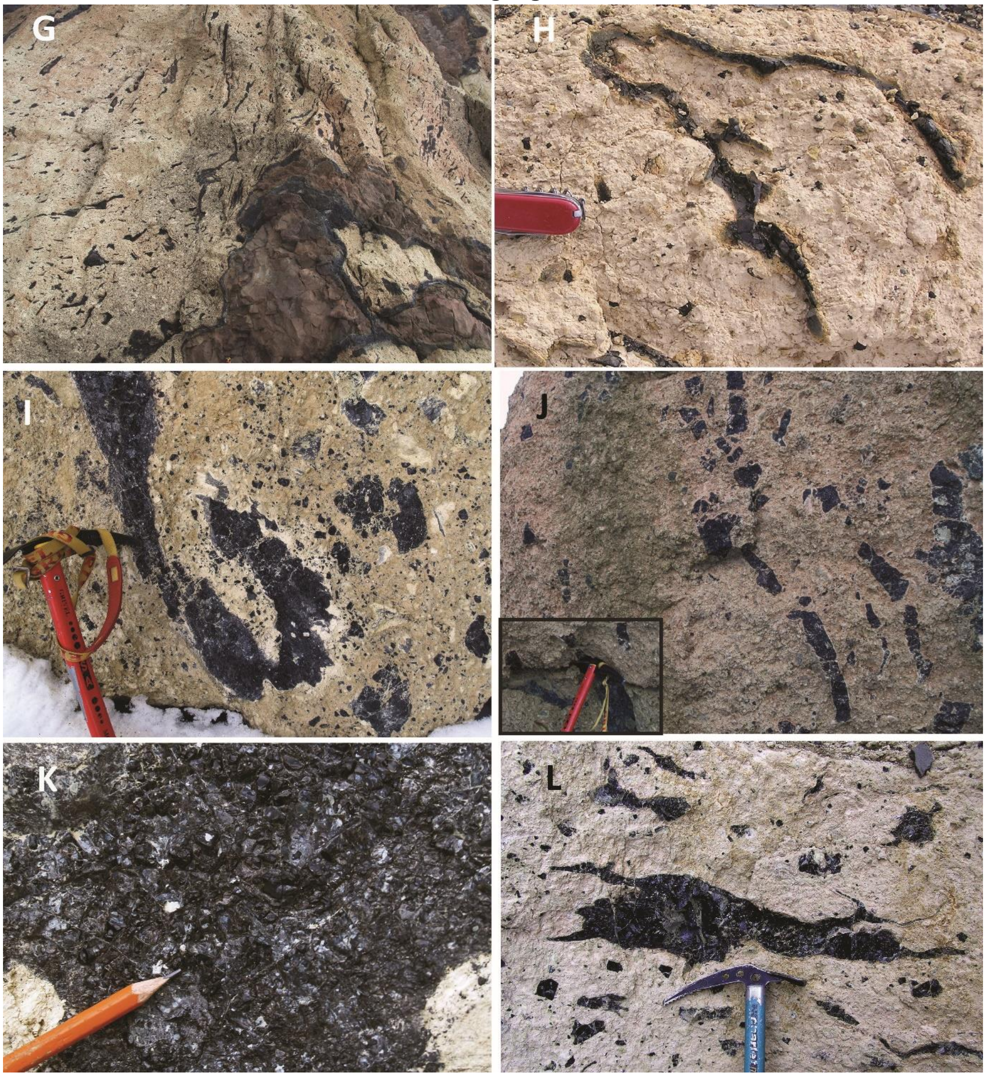

About 10-15 % of lithofacies B (based on visual estimates in the field and calculated from image analyses) is composed of outsize obsidian clasts, mostly 20-80 cm long but up to c. 2 m, and on average 6 cm thick. Their vesicularity is low to absent and the few vesicles present are variably flattened (ovoid/lenticular). They contain a textural zoning composed of alternating crystallite-rich and crystallite-free glass, the crystallites being decussate and arranged in small rosettes (Fig. 5e). The obsidian clasts appear thin and ribbon-like in two dimensions. However, on outcrop corners most appear to be disk-like (oblate) in three 5f). exposures suggest that at least some may have true ribbon shapes (Fig. They are all referred to as ribbons here, for convenience, since that is their dimensions, but the overwhelming appearance on the two-dimensional smooth rock faces. The ribbons are conspicuously orientated roughly parallel and dipping at c. 10-14° to the east. Although imbrication was not clearly identified, the basal surface of the deposit (and therefore the bedding orientation) is only minimally exposed. It is thus possible that the ribbons are extensively imbricated (c.f. Branney and Kokelaar 1992, fig. 4, and Branney and Kokelaar 2002, fig. 5.4C). Conversely, close to intrusions with highly irregular shapes, the obsidian clasts are re-orientated into much steeper attitudes (Figs 5g); other, more sheet-like intrusions simply cut across the obsidian clasts without deflecting them. Many obsidian clasts have fluidal shapes characterised by gentle folding but including examples that are folded back on themselves (Fig. 5h), and there is a gradation into fractured and broken ribbons that have separated into trails of angular fragments (Figs 5i, j). Many of the obsidian clasts are pervasively jigsaw-fractured on a sub-centimetre scale (Fig. 5k). Clast terminations vary from wispy, with curved tendril-like ends (Fig. 5l), to abrupt and angular where the ends have broken off (Figs 5j).

Trachytic intrusive member

The trachytic pyroclastic member contains abundant dark grey to grey-brown trachytic intrusions between 0.5 and 15 m thick, many with north to north-east trends (see also Wright-Grassham 1987). They dominate the upper half of Windscoop Bluff almost to the exclusion of pyroclastic lithofacies. The latter occur as a few thin screens between intrusions and are conspicuous by their much paler colour (Fig. 3). Contacts between the intrusions and the lapilli tuffs are often sharp but they vary from ill-defined (diffuse) to crenulated and peperitic. Intrusions with thick (10-20 cm) black glassy rims are only prominent where they cut lithofacies B. The glass is finely jigsaw-fractured and displaced fragments become progressively mingled with the enclosing lapilli tuff away from the intrusions. Most of the intrusions have conspicuously fluidal shapes (Fig. 5g) but some are more sheet-like (tabular). With the two-dimensional exposure of much of the outcrop, which is often orientated almost parallel to the intrusion walls, it is unclear whether the margins are quite as fluidal as they seem. At the very least, however, they indicate highly irregular margins that may be developing bulbous or pillow-like bulges.

Geochemistry

A representative analysis (OU78624) of the pumiceous lapilli in lithofacies B is provided in Table 1. The sample was prepared by removing the obsidian, the few lithic fragments and the ash matrix. It has a trachyte composition that, although peraluminous, is close to peralkalinity (Table 1, Fig. 6). Obsidian ribbons were also sampled at three locations within lithofacies B: a. near the basal contact (OU78706), b. middle of the unit (OU78707), and c. adjacent to the upper contact with the trachytic intrusive member (OU78712). Each sample was obtained approximately in a vertical transect (i.e. effectively equidistant from any inferred source). The three obsidian samples have very similar trachyte compositions (indistinguishable within error), but they are different (poorer in silica, and richer in alkalis) from the associated pumiceous lapilli (Fig. 6) and they are peralkaline [$((Na_2O+K_2O)/Al_2O_3)_{mol}$ 1.12-1.13]. The preservation of isotropic glass in thin section suggests these samples are essentially unaltered and that the difference in alkali contents is primary. A dyke from the intrusive member was also analysed and is also trachytic, but richer in silica and poorer in alkalis than any of the fragmental rocks analysed (Fig. 6).

Table 1 Geochemical analyses of Mason Spur trachytic rock and clast types.

	Lithofacies B matrix	Trachytic dyke	Spatter Clasts		
			a	b	c
OU #	OU78624	OU78628	OU78706	OU78707	OU78712
Field I.D.	309	322	314	341	339
Longitude	164° 32.751	164° 23.402	164° 32.596	164° 32.170	164° 32.337
Latitude	78° 32.848	78° 33.791	78° 32.875	78° 32.871	78° 32.947
Mg# (atom)	11.00	11.40	13.58	14.33	12.92
SiO_2	60.02	63.44	60.54	60.24	60.23
TiO_2	0.52	0.63	0.63	0.55	0.56
Al_2O_3	15.45	14.83	15.91	15.7	15.71
$Fe_2O_{3\ Total}$	8.98	7.39	-	-	-
FeO_{Total}	8.13	6.69	6.58	6.61	6.73
MnO	0.30	0.26	0.26	0.30	0.27
MgO	0.28	0.24	0.29	0.31	0.28
CaO	1.48	0.97	1.35	1.33	1.29
Na_2O	6.06	6.35	7.56	7.36	7.47
K_2O	4.93	5.05	5.00	5.00	5.00
P_2O_5	0.08	0.04	0.08	0.10	0.06
LOI	1.47	1.11	-	-	-
Total	99.12	99.94	98.57	97.87	97.97
FeO	4.49	3.70	3.66	3.67	3.74
Fe_2O_3	4.04	3.32	3.29	3.31	3.37
Na2O+K2O	10.99	11.40	12.56	12.35	12.47
$[(Na2O+K2O)/Al2O3]_{mol}$	0.99	1.07	1.12	1.12	1.13
Log η*	3.57	3.78	3.52	3.52	3.51

OU#: University of Otago catalogue number. Mg# = 100[Mg/(Mg+Fe)]. LOI: loss on ignition. η = viscosity calculated for T = 1273°K, H2O = 1.5 weight % and assuming no halogens (calculated after Giordano et al. 2008). The spatter clasts analyses were performed by electron microprobe technique. The matrix analysis and the trachyte dyke analysis were each performed by X-ray fluorescence technique. Quantitative error (accuracy + precision) for XRF Na_2O is c. 0.03% and for K_2O is 0.05% (Rousseau, 2001). Quantitative error (accuracy + precision) for major oxides determined by electron microprobe is 1-2% (e.g. Reed, 2005). The data from the two analytical sources, including errors, do not overlap and are statistically separated.

Discussion

Interpretation of lithofacies A: trachytic lapilli tuff (ignimbrite)

Lithofacies A is poorly sorted and mainly massive. Together with the abundance of pumice lapilli and variable proportion of ash matrix formed from broken pumices and shards, these features are inconsistent with an origin by fallout and the deposits are much more characteristic of ignimbrites, transported and deposited progressively by a granular-fluid-based current (Branney and Kokelaar 1992, 2002). There is no evidence of welding and the deposits must have been relatively cool (below sintering temperature; Valentine et al. 2000). The abundance of relatively coarse pumiceous lapilli and generally minor fine ash are consistent with a proximal or medial location relative to the source vent(s) (Valentine et al. 2000; Allen 2005; Bear et al. 2009a,b).

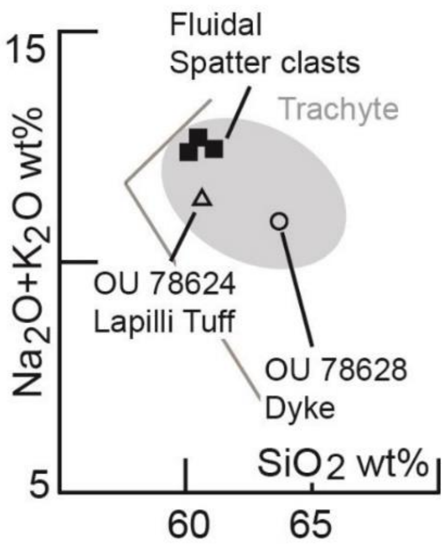

Fig. 5 Total Alkalis versus Silica (TAS) diagram (after Le Bas et al. 1986). The grey field encompasses the range of trachytic volcanic rock compositions from Mason Spur (Martin et al. 2013). Also shown are the compositions of individual obsidian spatter from the spatter-rich deposit (lithofacies B; squares), separated pumice lapilli from the associated matrix (triangle), and a coeval trachytic dyke (circle)

Interpretation of lithofacies B: trachytic spatter-rich lapilli tuff (ignimbrite)

Like lithofacies A, lithofacies B is also poorly sorted (matrix supported), dominated by pumiceous lapilli, massive and ungraded. It differs, however, in the additional presence of distinctive large ribbon- and (mainly) thin disk-shaped obsidian clasts and diffuse domains rich in angular, dense obsidian lapilli. Although the rocks are relatively poor in ash, the outsized obsidian ribbons are supported by a lapilli-rich matrix. Similar deposits with a complete absence of tractional stratification are generally inferred to have been associated with a pyroclastic current that was granular-fluid-based (Branney and Kokelaar 1992; Kokelaar et al. 2007), as we infer. This inference is supported by the numerous outsize (up to 2 m in length) obsidian ribbons which lack impact structures and which are significantly larger than associated juvenile pumices, suggesting a lack of hydraulic equivalence and, thus, lateral transport in a density current rather than by fall. Moreover, the denser obsidian ribbons are much larger than the associated less dense pumices, which is also anomalous for a fall deposit, and the basal contact is sharp and appears erosive. In summary, the fines-depletion, matrix support, massive nature, preferential alignment of the obsidian ribbons and erosive base suggest that the deposit was emplaced from a density current rather than by ballistic fallout. The lack of vertical size grading of the spatter clasts at Windscoop Bluff is different from that of other spatter-rich deposits (Mellors and Sparks 1991; Valentine et al. 2000). However, the upper contact of the deposit is intrusive and any grading which may have been present above that elevation is no longer exposed. The lack of any overall vertical and lateral grading pattern(s) in the deposit is also consistent with a very proximal location, i.e. within the caldera and probably close to its likely source (c.f. Kokelaar et al. 2007). With their evidence for plastic deformation indicative of emplacement in a hot state, the large obsidian ribbons are interpreted as spatter. Spatter is commonly produced ballistically during low-explosivity Strombolian eruptions or during periods of fire fountaining (Rader and Geist 2015). It is especially common in mafic magmas but much less so for more evolved compositions. Spatter is characteristic of low-viscosity magmas and consists of lapilli and bombs with fluidal shapes due to stretching and shearing during fragmentation, ejection and ballistic transport, many of which agglutinate on landing; they often have highly vesicular cores but can be dense (Giannetti and Luongo 1994; Sumner et al. 2005; Rader and Geist 2015). However, the shapes of the obsidians in lithofacies B differ from spatter normally associated with ignimbrites. The latter have subspherical, ellipsoidal, spindle, discoidal, fusiform, cauliform and highly irregular (amoeboid) shapes indistinguishable from bombs in subaerially erupted successions (Mellors and Sparks 1991; Branney and Kokelaar 2002), and they may also have chilled dense rinds with ropy or breadcrusted textures and vesicular interiors. By contrast, obsidian clasts in the Windscoop Bluff deposit appear to be both ribbon-like and strongly flattened disks and they are seemingly largely nonvesicular. Moreover, they show a progressive textural gradation into broken and disaggregated spatter not seen in other published examples. The apparent very low vesicularity in the Mason Spur spatter clasts may be due to strong flattening during stretching of a very fluid magma (see below) and a higher original vesicularity may have been present that is not now evident. Their surface features are uncertain because of a lack of suitable exposure but they appear more or less smooth when observed in profile (Fig. 5f). They are also not agglutinated. However, from the overall similarities, the deposit is interpreted as a fines-poor, spatter-rich ignimbrite. The ribbons suggest the pyroclastic flow was not highly turbulent, and without significant internal shearing, at the time of their incorporation.

The different shapes of the spatter in lithofacies B compared with those seen in other spatter-bearing ignimbrites are probably a function of the trachytic composition of the magma, which must have been very fluid at the time of eruption. The viscosity of trachytes is intermediate between viscous rhyolites and more fluid phonolites (Giordano et al. 2004). Rhyolites typically erupt explosively whereas phonolites are either effusive or explosive (Le Losq et al. 2015). At comparable eruptive temperatures, the viscosity of hydrous trachyte compositions can approach that of phonolites, suggesting that some trachytes may also erupt in a very fluid fashion, especially if they are peralkaline. Calculations of the viscosity (η) of the obsidian magma (crystal-free), based on the model of Giordano et al. (2008), show that it was very low (η = 3311 Pa s at T = 1273°K and H_2O = 1.5 weight %; the value assumes that fluorine, which will lower the viscosity, is absent (not analysed)). This estimate is empirical as the effective viscosity is an additive function of compositional and physical effects and there are many additional factors not included in the calculation, such as iron redox state, bubble densities and distributions (crystal densities and distributions seem to be negligible in these very crystal-poor magmas), temperature gradients, etc. (Le Losq et al. 2015). Indeed, a temporally heterogeneous spatial distribution of bubbles within a conduit can determine whether an eruption is explosive (Strombolian) or passive. The modelled obsidian magma viscosity is very similar to that calculated for the associated pumice composition (η = 3715, for similar conditions) but as we lack determinations for juvenile H_2O and halogens, there may be a greater dissimilarity than the calculated values suggest. The calculated viscosities are low and, because the obsidians are free of juvenile crystallites or microlites (those crystallites present are due to post-depositional devitrification), the fragmentation threshold for brittle failure may not have been reached during magma ascent (c.f. Papale 1999) consistent with the fluidal obsidian shapes. These observations agree with the findings of Allen (2005), who suggested that a relatively low-viscosity magma is required for explosive eruptions containing a combination of spatter and pumice.

Interpretation of the trachytic intrusive member

The intrusions in lithofacies A and B occur in two main forms: (i) highly irregular amoeboid fluidal shapes; and (ii) more regular and sheet-like, i.e. dykes with planar walls. The different morphologies suggest that at least two phases of intrusion took place, the first (irregular, amoeboid intrusions) being when the lapilli tuff host was unconsolidated and probably damp (to give the prominent glassy, sometimes brecciated margins of the intrusions); and the second (sheet-like intrusions) emplaced after consolidation and induration, with injection along brittle fractures. The lapilli tuff matrices of lithofacies A and B, and the crosscutting intrusions and spatter clasts in lithofacies B, are all trachytic and broadly similar compositionally (Fig. 6 and Table 1), although with small differences that may have significance for the mechanisms of mixing of the contrasting clast types (see section 6.5). However, the compositions and field relationships suggest that the fluidal-shaped intrusions, at least, were emplaced while the trachytic pyroclastic member was unconsolidated, and are thus coeval, suggesting a common magmatic source and a general genetic link with the host deposit.

Eruptive processes during generation of lithofacies B

The dynamics of peralkaline eruptions are poorly understood and have never been observed. They will be strongly influenced by the low magmatic viscosities and correspondingly low glass transition temperatures, which will prolong the duration of fluidity and plasticity of the juvenile clasts (Di Genova et al. 2013; Hughes et al. 2017). In lithofacies B, there is a gradation between plastically deformed obsidian clasts (Fig. 5h),

Table 2 Characteristics of lithofacies B (trachytic spatter-rich lapilli tuff). See text for discussion.

	Characteristic	**Interpretation**
Grain size	Poorly sorted	Rapid deposition from a *pdc
	Ash matrix	Fine fragmentation and rapid deposition
	Pumiceous lapilli supported	Proximal or medial location
	No vertical grading of size	May be artificial - upper deposit obscured by intrusions
Clast characteristics	Abundant fluidal spatter clasts	Hot emplacement. Clasts are stretched and sheared by overriding PDC
	No vertical or lateral grading of clast abundance	Constant rate of deposition
	No cracks in folded clasts	Absence of water during emplacement
	Fractured and broken spatter	Fracturing caused by rapid water cooling
	Lithic clasts very rare, lapilli size	No vent widening or caldera roof collapse & disintegration
	Glass in clasts is isotropic in thin section	Spatter clasts are unaltered
Deposit characteristics	Massive bedding	Rapid progressive aggradation from a density current
	'Nests' of blocky obsidian lapilli	Disintegration of spatter by fracturing caused by rapid cooling
	Trails of broken obsidian lapilli	Laminar flow in a shearing viscous current
	Diffuse domains rich in blocky obsidian lapilli	Disintegration of spatter by fracturing caused by rapid water cooling & inefficient dispersal by turbulent eddies
	Common orientation of spatter clasts	Lateral component to emplacement mechanism; possible imbrication
	Association of vesicle-poor spatter and pumice	No hydraulic equivalence; lateral transport
	Association of very large spatter and much smaller pumice	No hydraulic equivalence; lateral transport
Deposit geometry	Deposition on slopes less than the angle of repose	Lateral current flow
	Erosive base	Lateral current flow

*** pdc: pyroclastic density current**

through obsidian clasts with brittle fractures (Fig. 5i) to ribbons disrupted into trails of angular blocky fragments (Fig. 5j). The prevalence of slightly to conspicuously folded and deformed obsidian ribbons (Fig. 5f) suggests that many retained their heat sufficiently for ductile behaviour to dominate, consistent with a low thermal diffusivity of the juvenile clasts (Thomas and Sparks 1992). In relatively 'dry' density currents, large parts of the current probably retained an interstitial gaseous phase (juvenile gases and ingested heated air), which would have cushioned and insulated the clasts and reduced the cooling rate. Because of their much larger size, the ribbons would remain hot and ductile for longer than the much smaller pumice lapilli. Eventually however, sufficient cooling may have occurred for some to start breaking, perhaps as the glass transition was crossed, yielding the broken ribbons. Such a scenario might occur without necessarily requiring a significantly more rapid cooling rate than for the unbroken ribbons. Alternatively however, the fracturing and disaggregation of some obsidian spatter clasts might suggest that some obsidian ribbons were rapidly chilled. Similar brittle fracture and disintegration textures are very rarely observed in other occurrences of spatter-rich ignimbrites that only had a 'dry' gaseous phase in the current (Allen 2005; Kokelaar et al. 2007). In those examples, the constituent spatter clasts are coherent and lack signs of rapid chilling suggesting that some additional, possibly environmental, factor is involved in the Mason Spur example. The development of pervasive jigsaw-fit fractures (Fig. 5k) and disintegration into blocky angular clasts suggest a possible role for water, probably as steam. Both have a very high specific heat capacity and thermal conductivity compared with air, and could cause the fragmentation (Mattox and Mangan 1997; Zimanowski et al. 1997; White et al. 2003). With complete disaggregation in a moving unstable current, the clasts might become dispersed on a scale of a decimetre or possibly metres, but the occurrence of obsidian fragments as trails in lithofacies B probably reflects local viscous shear during laminar flow. The evidence for progressive disaggregation and shearing during flow indicates that any interaction with water occurred during transport rather than after deposition or in the vent (c.f. Valentine et al. 2000). This is also supported by the presence of diffuse 'domains' (i.e. patches with a high abundance of a particular clast type) composed of angular blocky nonvesicular obsidian fragments in the relatively coarse (pumice-lapilli-dominated) matrix supporting the spatter clasts; the domains are interpreted as the highly fragmented remains of obsidian ribbons that were frozen in place before they became completely dispersed.

The source of any water involved could be either patches of very wet (possibly puddled) ground, a stream, shallow lake or even snow crossed by the density currents, with the water vaporized and ingested as steam. Whilst the eruptive environment is only poorly known, evidence supporting a wet or damp milieu includes: (i) admittedly rare ash-coated lapilli in lithofacies A (Fig. 4c), implying a damp eruption column (Brown et al. 2012); (ii) several of the coeval intrusions have thick and locally brecciated glassy margins, implying intrusion into a damp unconsolidated lapilli tuff host; (iii) the margins of individual coeval intrusions vary from planar with thin or absent glassy selvages, to highly fluidal with thick glassy margins, suggesting that the host deposit may have been variably damp when intruded; and (iv) the reorientation of obsidian ribbons subvertically above the amoeboid intrusions (Fig. 5g) suggests either gas fluidization from within the ignimbrite or possibly localized fluidisation of an unconsolidated damp or wet host. On balance, a fluid phase, probably steam, is inferred to have been present in parts of the density current responsible for lithofacies B and led to fracturing and disintegration of some of the obsidian spatter. Many other obsidian spatter clasts deformed plastically without fracturing, probably due to insulation by a 'dry' gas phase, with its low thermal diffusivity (Kokelaar et al. 2007). Thus, an inhomogeneous density current is envisaged, comprising diffuse, ill-defined and probably short-lived domains dominated either by 'dry' gases or by steam. Table 2 summarises the salient features of pyroclastic lithofacies B and its interpretation.

Mixing mechanisms

Various mechanisms and processes have been invoked in the literature to explain the combination of spatter and pumice in pyroclastic deposits. They include:

1. Mingling of pumice and spatter in a single vent prior to being ejected simultaneously in a plume that collapses to form a pyroclastic deposit (e.g. Mellors and Sparks 1991; Valentine et al. 2000; Kokelaar et al. 2007);
2. The coexistence and mingling of a spatter fountain and an explosive eruption plume, sourced in different vents but depositing together (e.g. Furukawa and Kamata 2004; Allen 2005); or
3. The collapse of over-steepened upper cone slopes due to rapidly accumulating deposits from Strombolian eruptions (e.g. Valentine et al. 2000).

At Mason Spur, the spatter clasts and their pumiceous lapilli tuff host deposit (lithofacies B matrix) are interpreted as being the products of a single volcanic episode, albeit with eruption not necessarily from a single vent. The angle of the palaeo-slope of lithofacies B is indicated by the consistent dip of the spatter clasts and the basal contact of the unit at c. 12°. This is much lower than the angle of repose. Moreover, the bulk of the deposit is composed of pumiceous lapilli with an ash matrix, unlike the clast make-up of a Strombolian cone. It is, therefore, unlikely that lithofacies B was created by the collapse of an over-steepened upper cone surface. Additionally, the small but distinct compositional differences between the co-existing obsidian and pumiceous clasts does not support simultaneous derivation from a single magmatic source and mingling of spatter and pumice within a shared vent. Rather, the intimate association of brittle and ductile obsidians with pumiceous lapilli supports a model of concurrent ballistic spatter fountaining and incorporation within overriding pyroclastic density currents.

Spatter-rich ignimbrites have been described elsewhere (e.g. Santorini: Mellors and Sparks 1991; Campei Flegrei: Scarpati et al. 1993, Perrotta and Scarpati 1994, Rosi et al. 1996; and Colorado: Valentine et al. 2000). However, they lack the textural gradation into the broken and disaggregated spatter seen at Mason Spur and inferred here to be caused by localised water interaction. Other examples of spatter-rich ignimbrites are also usually rich in lithic clasts (e.g. Rosi et al. 1996; Valentine et al. 2000; Allen 2005; Kokelaar et al. 2007; Bear et al. 2009a,b). The lack of any direct association between the occurrences of spatter clasts with coarse breccia layers at Mason Spur suggests that the generation and incorporation of the spatter was unrelated to an increase in current competence caused by fluctuating vent conditions or flow unsteadiness. The presence of the spatter appears to be an intrinsic feature of the current, either when it formed or else added at a later stage, when spatter mingled with the current. Spatter is emplaced ballistically, hence the mingling of fluidal spatter with volumetrically dominant pumices implies the incorporation of ballistic clasts in a pyroclastic density current and the co-emplacement of magmas that are gas-poor and gas-rich, relative to one another. The presence of obsidian ribbons throughout the pumice-rich deposit, except for the basal 1-2 m, suggests that the spatter fountain persisted during the period of collapsing eruption plume that generated the enclosing pumiceous ignimbrite, apart from the earliest flow stage.

For magma utilising a single vent, it has been suggested that the magma may experience fluctuations in the rise rate that include a period of magma rise that is faster than bubble nucleation and coalescence. This has been cited as a possible mechanism for temporarily producing spatter within an explosive eruption of vesiculating magma (Bear et al. 2009b). Slower magma rise rates would allow the formation of bubbles and produce much more highly vesiculated magma and abundant pumice. Alternatively, influx of external water might also be involved (Houghton and Wilson 1989; Mellors and Sparks 1991; Valentine et al. 2000). Mellors and Sparks (1991) suggested that a pre-existing lake of degassed lava is required together with an influx of water to trigger ejection of the spatter.

Failure of the magma chamber roof is another possible solution. If, in the process, the lithostatic pressure falls below the magma pressure, it may trigger an explosive spatter-forming eruption of deeper undegassed magma that is driven by magmatic overpressure and not volatile expansion (Perrotta and Scarpati 1994). Spatter clasts are then sprayed into the pyroclastic density current created by the coeval collapsing eruption column. Possible support for this model is provided by the observation that obsidian spatter is absent in the basal 1-2 m of the deposit, indicating an early eruptive stage dominated by column collapse and in which a spatter 'event' was absent. Conversely, an *increase* in lithostatic load has also been implicated, caused by roof collapse during climactic eruption phases and a dramatic increase in magma discharge (Allen 2005). However, models involving roof collapse have problems: (1) caldera roof collapse typically generates abundant lithic clasts (e.g. Druitt and Sparks 1982; Druitt and Sparks 1984; Rosi et al. 1996; Allen 2005; Bear et al. 2009b). Such an explanation appears to be inapplicable to lithofacies B unless the collapsing roof failed to break up (probably an unusual event); and (2) it is hard to see why co-eruption of undegassed or poorly degassed magma should not rapidly vesiculate during its ejection, resulting in significantly vesiculated spatter (such as were described by Allen 2005, and Bear et al. 2009b; but see Branney and Kokelaar 2002).

The conspicuous absence of a basal pumice fall deposit at Mason Spur suggests that the eruption plume may have collapsed before it became buoyant (c.f. Allen 2005). Premature plume collapse is commonly attributed to an effect of vent widening or to a reduction in volatile content leading to lower volatile-induced vent exit speeds and reduced buoyancy, resulting in a magma chamber erupting by 'boiling over', a low eruption column and ejection of spatter (Woods 1995; Bear et al. 2009b). The absence of lithic debris argues against a vent-widening mechanism and the abundance of highly vesicular pumice is inconsistent with a lower volatile content. Other explanations are even more problematical to assess and include rapid changes in the depth of magmatic evacuation (Branney and Kokelaar 2002; Dávila-Harris et al. 2013) or contrasting magma residence times leading to density variations (Sable et al. 2006; Shea et al. 2012).

Conversely, *multiple* vents may be involved, with varying eruption styles and intensities ranging from Plinian to lava fountaining (Mellors and Sparks 1991; Rosi et al. 1996; Valentine et al. 2000; Watkins et al. 2002). The spatter from one vent may become mixed with pumiceous ignimbrite sourced in another vent as the density current flows across the surface. This scenario is supported by the compositional difference observed between the constituent pumice lapilli and spatter clasts, which might imply different magma chambers or two vents tapping different levels of a single compositionally stratified chamber (Rosi et al. 1996). However, the combination of strong contrasts in vesicularity between the pumice lapilli and obsidian ribbons and the compositional differences are most easily explained as a result of eruptions from two magma chambers.

In summary, the simplest explanation for the formation of lithofacies B, and the one which we prefer, is broadly that proposed by Rosi et al. (1996). It involves co-eruption at two different vents, one involving explosive fragmentation of a gas-rich magma, development of a low eruption column and column collapse generating a pyroclastic density current, whilst the other vent was characterised by lava fountaining which created much coarser pyroclasts of fluidal trachytic spatter. Mingling of the two very different pyroclastic products (ignimbritic pumiceous lapilli and ash; vesicle-poor ballistic spatter) took place where the spatter fountain was overrun by the pyroclastic density current (Figure 7). Without the addition of spatter, only lithofacies A ignimbrite would be deposited. Because only a single outcrop of lithofacies B has been observed at Mason Spur, it appears that the co-eruption of two vents tapping separate trachytic magmas was a very rare event. The additional ingestion of small amounts of surface water is inferred to be responsible for the distinctive textural features of some of the spatter pyroclasts.

Synthesis and conclusions

A distinctive Neogene (c. 12 Ma), trachytic, spatter-rich pyroclastic density current deposit (ignimbrite) > 80 m thick (lithofacies B) was studied at Mason Spur, Antarctica. It forms part of a very thick (hundreds of metres) caldera-filling unit (trachytic pyroclastic member) dominated by other trachytic ignimbrites and breccias (lithofacies A), and abundant coeval trachytic intrusions (trachytic intrusive member). Key field characteristics of the studied ignimbrite include the following: a) conspicuous fluidal black obsidian spatter up to 2 m long supported in a pale pumiceous lapilli tuff matrix; b) spatter clasts that are spectacularly ribbon-like in cross-section but have predominantly flattened disk shapes; c) poor sorting and a lack of size grading in the matrix; d) apart from a paucity of spatter in the basal 1-2 m, no vertical or lateral grading of spatter

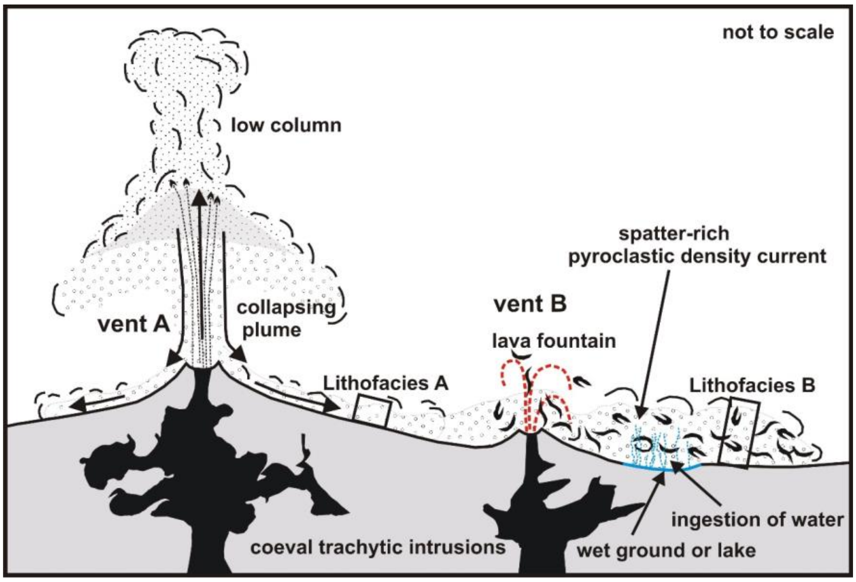

Fig. 7 Schematic diagram illustrating how the spatter-rich ignimbrite at Mason Spur might have formed. Eruptions are envisaged at two separate vents that tapped different trachytic magma batches, one (A) creating pumiceous ignimbrite, the other (B) creating highly fluidal spatter in a lava fountain. Mingling of the spatter took place when vent B was overrun by the pyroclastic density current sourced in vent A, resulting in a compound ignimbritic lithofacies (lithofacies B). Without the addition of spatter, only lithofacies A would be deposited.

abundance; e) massive bedding; f) common orientation of spatter clasts at an angle less than the angle of repose; (g) erosive base; and (h) the spatter and pumiceous lapilli have slightly different (trachytic) compositions. Lithofacies B was rapidly erupted onto a gently dipping (c. 12°) palaeo-surface that probably included either patches of wet ground (possibly puddled), a stream, a shallow lake or possibly snow. Water was ingested by the overflowing pyroclastic density current, as steam, and caused brittle fracture of some spatter, many clasts of which disintegrated to form diffuse patches rich in lapilli-size obsidian fragments, but most spatter escaped profound fracturing and retained a fluidal shape. Although several general models have been proposed for the origin of spatter-rich ignimbrites, the simplest (and our favoured) interpretation for lithofacies B involves the eruption of hot, dense spatter and pumiceous lapilli tuff from two separate co-eruptive vents, with mingling of the contrasting pyroclast types taking place when spatter clasts from a lava fountain were entrained in a pyroclastic density current independently sourced in a low collapsing plume. The distinctive highly attenuated shapes of the spatter, with relatively smooth surfaces, are probably a consequence of the trachytic spatter-forming magma being very fluid, which resulted in it acting like more fluidal phonolite.

Acknowledgements This project was supported by a NZARI Research Project award (NZARI 2016-1-1) and APM is grateful for an Antarctica New Zealand (New Zealand Post) scholarship. The authors are also grateful to all the staff at Scott Base, field assistants Matt Windsor, Benji Nicholson and John Cottle, and Sean Mullally ('Snow') and Andrew Hefford (pilots for Southern Lakes Helicopters) for their excellent logistical support during the 2005-06 and 2016-17 field seasons when the fieldwork for this project was carried out. We are also very grateful for conversations with Nina Jordan (Leicester University) about the characteristics and style of eruptions of peralkaline felsic ignimbrites, and Kelly Russell (University of British Columbia) for his invaluable help calculating viscosities. We thank journal reviewers R. Cas and M. Rosi and associate editor P.-S. Ross for their comments on the manuscript.

References

Allen SR (2005) Complex spatter- and pumice-rich pyroclastic deposits from an andesitic caldera-forming eruption: the Siwi pyroclastic sequence, Tanna, Vanuatu. Bull. Volcanol. 67:27-41

Bear AN, Cas RAF, Giordano G (2009a) The implications of spatter, pumice and lithic clast rich proximal co-ignimbrite lag breccias on the dynamics of caldera forming eruptions: The 151 ka Sutri eruption, Vico Volcano, Central Italy, J. Volcanol. Geotherm. Res. 181:1-24

Bear AN, Cas RAF, Giordano G (2009b) Variations in eruptive style and depositional processes associated with explosive, phonolitic composition, caldera-forming eruptions: The 151 ka Sutri eruption, Vico Caldera, central Italy. J. Volcanol. Geotherm. Res. 184(3):225-255

Branney M, Kokelaar P (1992) A reappraisal of ignimbrite emplacement: progressive aggradation and changes from particulate to non-particulate flow during emplacement of high-grade ignimbrite. Bull. Volcanol. 54(6):504-520

Branney MJ, Kokelaar P (2002) Pyroclastic density currents and sedimentation of ignimbrites. Geo. Soc. Mem. 27:1–138

Brown RJ, Bonadonna C, Durant AJ (2012) A review of volcanic ash aggregation. Phys. Chem. Earth 45-46: 65-78

Dávila-Harris P, Ellis BS, Branney MJ, Carrasco-Núñez G (2013) Lithostratigraphic analysis and geochemistry of a vitric spatter-bearing ignimbrite: the Quaternary Adeje Formation, Cañadas volcano, Tenerife. Bull. Volcanol. 75(6):1-15

Di Genova D, Romano C, Hess KU, Vona A, Poe BT, Giordano D, Dingwell DB, Behrens H (2013) The rheology of peralkaline rhyolites from Pantelleria Island. J. Volcanol. Geotherm. Res. 249:201-216

Druitt TH, Sparks RSJ (1982) A proximal ignimbrite breccia facies on santorini , Greece. J. Volcanol. Geotherm. Res. 13(1):147-171

Druitt TH, Sparks RSJ (1984) On the formation of calderas during ignimbrite eruptions. Nature 310(5979):679-681

Elliot DH, Hanson RE (2001) Origin of widespread, exceptionally thick basaltic phreatomagmatic tuff breccia in the Middle Jurassic Prebble and Mawson Formations, Antarctica. J. Volcanol. Geotherm. Res. 111:183-201
Furukawa K, Kamata H (2004) Eruption and emplacement of the Yamakogawa Rhyolite in central Kyushu, Japan: A model for emplacement of rhyolitic spatter. Earth Planets Space 56:517-524
Giannetti B, Luongo G (1994) Trachyandesite scoria-flow and associated trachyte pyroclastic flow and surge at Roccamonfina Volcano (Roman Region Italy). J. Volcanol. Geotherm. Res. 59:313-334
Giordano D, Romano C, Papale P, Dingwell DB (2004) The viscosity of trachytes, and comparison with basalts, phonolites, and rhyolites. Chem. Geol. 213(1):49-61
Giordano D, Russell JK, Dingwell DB (2008) Viscosity of magmatic liquids: A model. Earth Planet. Sci. Lett. 271(1):123-134
Houghton BF, Wilson CJN (1989) A vesicularity index for pyroclastic deposits. Bull. Volcanol. 51:451-462
Hughes EC, Neave DA, Dobson KJ, Withers PJ, Edmonds M (2017) How to fragment peralkaline rhyolites: Observations on pumice using combined multi-scale 2D and 3D imaging. J. Volcanol. Geotherm. Res. 336:179-191
Kokelaar P, Raine P, Branney MJ (2007) Incursion of a large-volume, spatter-bearing pyroclastic density current into a caldera lake: Pavey Ark ignimbrite, Scafell caldera, England. Bull. Volcanol. 70:23-54
Kyle PR (1990) McMurdo Volcanic Group - western Ross Embayment: Introduction. In: LeMasurier WE, Thompson J (eds) Volcanoes of the Antarctic plate and southern oceans. Antarctic Research Series 48:18-25
Le Bas M, Maitre MJ, Streckeisen A, Zanettin B (1986) A chemical classification of volcanic rocks based on the total alkali-silica diagram. J. Petrol. 27:745-750
Le Losq C, Neuville DR, Moretti R, Kyle PR, Oppenheimer C (2015) Rheology of phonolitic magmas – the case of the Erebus lava lake. Earth Planet. Sci. Lett. 411:53-61
LeMasurier WE (1990) Late Cenozoic Volcanism on the Antarctic Plate: An Overview. In: LeMasurier WE, Thomson JW (eds) Volcanoes of the Antarctic Plate and Southern Oceans. American Geophysical Union, Washington, pp 1-17
Martí J, Geyer A, Aguirre-Diaz G (2013) Origin and evolution of the Deception Island caldera (South Shetland Islands, Antarctica). Bull. Volcanol. 75(6):732
Martin AP (2009) Mount Morning, Antarctica: Geochemistry, geochronology, petrology, volcanology, and oxygen fugacity of the rifted Antarctic lithosphere. PhD thesis (geology). Department of Geology. University of Otago, Dunedin, 264 p
Martin AP, Cooper AF (2010) Post 3.9 Ma fault activity within the West Antarctic rift system: onshore evidence from Gandalf Ridge, Mount Morning eruptive centre, southern Victoria Land, Antarctica. Antarct. Sci. 22:513-521
Martin AP, Cooper AF, Dunlap WJ (2010) Geochronology of Mount Morning, Antarctica: Two-phase evolution of a long-lived trachyte-basanite-phonolite eruptive center. Bull. Volcanol. 72:357-371, doi: 310.1007/s00445-00009-00319-00441
Martin AP, Cooper AF, Price RC (2013) Petrogenesis of Cenozoic, alkalic volcanic lineages at Mount Morning, West Antarctica and their entrained lithospheric mantle xenoliths: Lithospheric versus asthenospheric mantle sources. Geochim. Cosmochim. Acta 122:127-152
Martin AP, Price RC, Cooper AF, McCammon CA (2015) Petrogenesis of the Rifted Southern Victoria Land Lithospheric Mantle, Antarctica, Inferred from Petrography, Geochemistry, Thermobarometry and Oxybarometry of Peridotite and Pyroxenite Xenoliths from the Mount Morning Eruptive Centre. J. Petrol. 56(1):193-226
Mattox TN, Mangan MT (1997) Littoral hydrovolcanic explosions: A case study of lava-seawater interaction at Kilauea Volcano. J. Volcanol. Geotherm. Res. 75:1-17
Mellors RA, Sparks RSJ (1991) Spatter-rich pyroclastic flow deposits on Santorini, Greece. Bull. Volcanol. 53:327-342
Panter K, McIntosh W, Smellie J (1994) Volcanic history of Mount Sidley, a major alkaline volcano in Marie Byrd Land, Antarctica. Bull. Volcanol. 56(5):361-376
Papale P (1999) Strain-induced magma fragmentation in explosive eruptions. Nature 397(6718):425-428
Parfitt EA, Wilson L (1995) Explosive volcanic eruptions—IX. The transition between Hawaiian-stye lava fountaining and Strombolian explosive activity. Geophys. J. Intl. 121: 226-232
Perrotta D, Scarpati C (1994) The Dynamics of the Breccia Museo eruption (Campi Flegrei Italy) and the significance of spatter clasts associated with breccias. J. Volcanol. Geotherm. Res. 59:335-355
Rader E, Geist D (2015) Eruption conditions of spatter deposits. J. Volcanol. Geotherm. Res. 304:287-293

Reed SJB (2005) Electron Microprobe Analysis and Scanning Electron Microscopy in Geology. Cambridge University Press, Cambridge, 189 pp

Roobol MJ, Smith AL, Wright JV (1987) Lithic breccias in pyroclastic flow deposits on St. Kitts, West Indies. Bull. Volcanol. 49:696-707

Rosi M, Vezzoli L, Aleotti P, De Censi M (1996) Interaction between caldera collapse and eruptive dynamics during the Campanian Ignimbrite eruption, Phlegraean Fields, Italy. Bull. Volcanol. 57(7):541-554

Rousseau RM (2001) Detection limit and estimate of uncertainty of analytical XRF results. Rigaku J. 18:33-47.

Sable JE, Houghton BF, Del Carlo P, Coltelli M (2006) Changing conditions of magma ascent and fragmentation during the Etna 122 BC basaltic Plinian eruption: Evidence from clast microtextures. J. Volcanol. Geotherm. Res. 158(3–4):333-354

Scarpati C, Cole PD, Perrotta D (1993) The Neapolitan Yellow Tuff - a large volume multiphase eruption from Campi Flegrei, southern Italy. Bull. Volcanol. 55:343 - 356

Shea T, Gurioli L, Houghton B (2012) Transitions between fall phases and pyroclastic density currents during the AD 79 eruption at Vesuvius: building a transient conduit model from the textural and volatile record. Bull. Volcanol. 74(10):2363-2381

Smellie J, López-Martínez J (2002) Text and geological and geomorphological maps. BAS GEOMAP series, Sheets 6-A and 6-B, Scale 1: 25 000. Geology and geomorphology of Deception Island. British Antarctic Survey, Cambridge, 77 p

Sumner JM, Blake S, Matela RJ, Wolff JA (2005) Spatter. J. Volcanol. Geotherm. Res. 142(1–2):49-65

Thomas RME, Sparks RSJ (1992) Cooling of tephra during fallout from eruption columns. Bull. Volcanol. 54(7):542-553

Trigila R, Walker GPL (1986) The Onano spatter flow, Italy: Evidence for a new ignimbrite depositional mechanism. Abstract. In: International Volcanological Congress. New Zealand, p 81

Valentine GA, Perry FV, WoldeGabriel G (2000) Field characteristics from spatter-rich density currents at Summer Coon Volcano, Colorado. J. Volcanol. Geotherm. Res. 104:187-199

Watkins S, Giordano G, Cas R, De Rita D (2002) Emplacement processes of the mafic Villa Senni Eruption Unit (VSEU) ignimbrite succession, Colli Albani volcano, Italy. J. Volcanol. Geotherm. Res. 118(1):173-203

White JDL, Houghton BF (2006) Primary Volcaniclastic Rocks. Geology 34:677-680

White JDL, Smellie JL, Clague DA (2003) Introduction: A Deductive Outline and Topical Overview of Subaqueous Explosive Volcanism. In: Explosive Subaqueous Volcanism. American Geophysical Union, pp 1-23

Woods AW (1995) The dynamics of explosive volcanic eruptions. Rev. Geophys. 33(4):495-530

Woods AW (2013) Sustained explosive activity: volcanic eruption columns and hawaiian fountains. In Fagents SA, Gregg TKP, Lopez RMC (eds) The physics and mathematics of volcanism. Cambridge |University Press, Cambridge, pp. 153-172

Wright-Grassham AC (1987) Volcanic geology, mineralogy, and petrogenesis of the Discovery Volcanic Subprovince, Southern Victoria Land, Antarctica. PhD thesis (geology). New Mexico Institute of Mining and Technology, 460 pp

Zimanowski B, Büttner R, Lorenz V, Häfele H-G (1997) Fragmentation of basaltic melt in the course of explosive volcanism. J. Geophys. Res-Sol. Ea. 102(B1):803-814